Wiley
Journal of Chemistry
Volume 2024, Article ID 7703829, 19 pages
https://doi.org/10.1155/2024/7703829

Research Article

Evaluation of the Potential of *Daucus crinitus* Extracts and Their Synthesized ZnO Nanoparticles in Inhibiting the Corrosion of Carbon Steel

Hatem Beddiar,[1] Sameh Boudiba,[2] Merzoug Benahmed,[3] Karima Hanini,[2,3] Alfred Ngenge Tamfu,[4] Louiza Boudiba,[2] Habiba Soltani,[1,2] Hocine Laouer,[5] and Salah Akkal[6]

[1]*Laboratory of Organic Materials and Heterochemistry, Echahid Cheikh Larbi Tebessi University, Constantine Road, Tebessa 12002, Algeria*
[2]*Laboratory of Applied Chemistry and Renewable Energies (LACRE), Echahid Cheikh Larbi Tebessi University, Tebessa, Algeria*
[3]*Laboratory of Bioactive Molecules and Applications, Faculty of Exact Sciences, Natural and Life Sciences, Echahid Cheikh Larbi Tebessi University, Constantine Road, Tebessa 12002, Algeria*
[4]*Department of Chemical Engineering, School of Chemical Engineering and Mineral Industries, University of Ngaoundere, Ngaoundere 454, Cameroon*
[5]*Laboratory for the Valorization of Natural Biological Resources, Ferhat Abbas University, Setif, Algeria*
[6]*Laboratory of Phytochemistry, Physicochemical and Biological Analyses, Mentouri University, Ain El Bey Road, Constantine 25000, Algeria*

Correspondence should be addressed to Alfred Ngenge Tamfu; macntamfu@yahoo.co.uk

Received 3 January 2024; Revised 7 May 2024; Accepted 13 May 2024; Published 30 May 2024

Academic Editor: Liviu Mitu

This study explores *Daucus crinitus* extracts (DCE) and zinc oxide nanoparticles (ZnO-NPs) synthesized using the extracts as corrosion inhibitors for carbon steel (CS) in HCl medium. The synthesized ZnO-NPs were characterized via UV-vis spectroscopy, exhibiting a peak at approximately 375 nm. The study employed weight loss (WL) and electrochemical measurements, alongside spectrophotometric evaluation of corrosion products. Surface morphology was assessed via scanning electron microscopy coupled with energy dispersive spectroscopy (SEM-EDS). Thermodynamic analysis revealed the physical adsorption of DCE on CS according to the Freundlich adsorption isotherm. Potentiodynamic polarization (PP) measurements indicated DCE as a mixed-type corrosion inhibitor. Electrochemical impedance spectroscopy (EIS) exhibited increased charge transfer resistance and reduced double-layer capacitance with inhibitory addition. The most effective inhibition was observed with butanol extract (BE) and improved more with its corresponding nanoparticles (BENPs), exhibiting inhibitory efficiencies of 80.20% and 91.20%, respectively, at 298 K with a concentration of 800 ppm. The evaluation of corrosion products using colorimetry revealed that the concentration of polyphenols decreased after the inhibitory process. Furthermore, the intensity of ferrous ions (Fe^{2+}) decreased as the inhibitory concentration increased. In addition, SEM-EDS analysis confirmed the presence of ZnO-NPs, which enhanced the surface morphology and established a protective layer formed by the adsorbed inhibitors. The SEM-EDS analysis confirmed the presence of ZnO-NPs, the enhancement of surface morphology, and the establishment of a protective layer formed by the adsorbed inhibitors.

1. Introduction

Renowned for its outstanding quality, mechanical characteristics, and cost-effectiveness, carbon steel is an important alloy that finds enormous use in manufacturing as a building material for reactors, storage, heat exchangers, and boilers, in addition to oil and gas transportation pipes [1]. However, this wide use makes it exposed to corrosion damage. To solve this problem, protection against this phenomenon is crucial and has acquired remarkable academic and industrial

attention [2–6]. It is to highlight that, among many methods used to fight against corrosion, the addition of inhibitors is often employed. Usually, organic products suggest good properties as inhibitors contained in their structure π bonds and heteroatoms in particular N, O, and S as constituent elements, and their inhibitory ability is attributed to their adsorption onto metal surfaces, forming a protective layer. Among these inhibitors, synthetic ones have good inhibitory efficiency [7–10], but they are limited due to their dangerous implications for the environment. Therefore, natural products were investigated due to their biodegradability, nontoxic properties, and absence of heavy metals [3, 11].

Recently, plants have become an important source of corrosion inhibitors for metal protection in acidic media as an alternative to synthetic chemicals frequently used [12]. Many papers reported the use of different parts of plants such as leaves (*Psidium guajava* Linn) [13], flowers (*Cytisus multiflorus*) [14], fruits (*Garcinia cambogia*) [15], seeds (*Azadirachta indica*) [16], aerial parts (*Equisetum arvense*, *Taxus baccata*, *Echium italicum* L.) [17–19], or even roots (*Solanum tuberosum*) [20] as eco-friendly inhibitors. These inhibitory properties are related to polyphenols, terpenoids, alkaloids, and so on [21]. Nanotechnology was introduced to enhance the inhibitory efficiency of these products [22, 23]. Recently, the research aims to develop biosynthesized nanoparticles using various plant extracts, as they contain molecules with electron-rich atoms that are able to form metallic nanoparticles with better corrosion inhibitory properties [24, 25]. According to the literature, ZnO-NPs showed remarkable biological properties, were environmentally harmless, and had low expenses [26, 27]. To the author's knowledge, *Daucus crinitus* has not previously been used for corrosion-inhibitive studies. It should be noted that previous studies on this species report the evaluation of the antioxidative properties of the phenolic extracts from its aerial parts [28], and antibacterial and the antifungal powers of its volatile oils [29–31].

This study aims to investigate the effectiveness of *Daucus crinitus* extracts as corrosion inhibitors and synthesize zinc oxide nanoparticles (ZnO-NPs) for testing their efficiency as inhibitors for carbon steel in an acidic environment. The investigation employs a combination of gravimetric and electrochemical techniques to assess corrosion inhibitory efficacy. Additionally, SEM-EDS analysis is conducted to characterize the surface morphology of the steel. To support the obtained results and better visualize them, a comparison of the solution composition (phenolic content and generated ferrous ion) before and after immersion in the carbon steel was carried out.

2. Materials and Methods

2.1. Plant Collection and Extraction. The aerial parts of *Daucus crinitus* were collected from the Algerian North East (Setif) during the flowering period. The plant material was identified by Dr. H. Laouer from the Laboratory for the Valorization of Natural Biological Resources at Ferhat Abbas University in Setif, Algeria. The plant material was dried in the shade and then submerged in a 70% methyl alcohol aqueous solution at room temperature for 24 hours. The mixture was filtered, and the remaining liquid was evaporated under reduced pressure. The obtained residue was dissolved in boiled water to remove chlorophyll and stored for 24 hours. After filtration, the solution was subjected to liquid-liquid extraction using three different solvents: methyl dichloride, ethyl acetate, and *n*-butanol. This process separates the components of the solution based on their polarity and solubility in different solvents, resulting in three different extracts: methylene dichloride extract (MDE), ethyl acetate extract (EAE), and *n*-butanol extract (BE) [32, 33].

2.2. Green Synthesis of Zinc Oxide Nanoparticles (ZnO-NPs) and UV-Vis Characterization. ZnO-NPs were synthesized using DCE following the literature description [34]. Specifically, 2 g of zinc nitrates $Zn(NO_3)_2{\cdot}6H_2O$ was solubilized in 50 mL of each extract solution (at a concentration of 1200 ppm) and subjected to constant stirring. Once complete dissolution was achieved, the mixture was heated to a temperature range of 60°C to 80°C until a yellowish precipitate formed. Subsequently, the solution underwent filtration, and the resulting solid was dried. The residue was calcinated at 400°C for one hour, resulting in the production of a white powder comprising ZnO-NPs. The UV-visible absorption spectra of the ZnO nanoparticles prepared using the three different extracts were recorded at room temperature within the range of 250–800 nm wavelength on a UV-vis spectrophotometer (Hitachi, U-3010).

2.3. Material Preparation. The CS used in this study, namely, API 5L-X60, possesses the following composition: carbon (0.26 wt%), manganese (1.35 wt%), phosphorus (0.03 wt%), and sulfur (0.03 wt%), with the remainder being iron. For weight loss tests, samples of CS are 1 cm^3, but for electrochemical measurements, a single facet of 1 cm^2 is used as a working electrode, covering the rest with epoxy resin. Before each test, substrates were sanded with emery paper (grades 400, 600, 800, 1200, 1500, and 2000), washed with distilled water, cleaned with acetone, then rinsed again with distilled water, and dried. The corrosive solution was hydrochloric acid (1 M) diluted from 37% HCl (Merck) with bidistilled water. Different MDE, EAE, and BE concentrations ranging from 0 to 1200 ppm with an increment of 100 ppm were utilized as inhibitors.

2.4. Total Phenolic Content (TPC). TPC estimation was employed using the Folin–Ciocalteu reagent following the Legwalia procedure [35]. Gallic acid was used as a reference for the calibration curve, and TPC values were expressed in gallic acid equivalents (μg GAE mg/mg extract).

2.5. Phenanthroline Method for Fe (II) Determination. This method [36] determines the dissolved ferrous ion (Fe^{2+}) concentration. In a 50 mL flask containing 3 mL of test solution, 1 mL of hydroxylamine hydrochloride solution (100 g/L) was added to reduce the existing Fe^{3+} to Fe^{2+}, followed by 4 mL of 1,10-phenanthroline (1 g/L) and 5 mL of

sodium acetate buffer (1.2 M at pH = 3.5), then completed with distilled water. After 10 min, the solution turned red, and subsequently, the absorbance was recorded at 510 nm. The employed iron standard solution was ferrous ammonium sulfate hexahydrate ($Fe(NH_4)_2(SO_4)_2{\cdot}6H_2O$). The formed complex follows the equation:

$$Fe^{2+} + 3\,o\text{-Phen} \longrightarrow Fe(o\text{-Phen})_3{}^{2+}. \quad (1)$$

The phenanthroline method was employed to quantify Fe^{2+} in the residual test solutions at optimal concentrations of DCE and NPs. A standard iron solution of ferrous ammonium sulfate hexahydrate was employed for calibration.

2.6. Weight Loss Measurements. In a 50 mL beaker containing 30 mL of the test solution (1 M HCl and DCE with various ratios), CS cubes were immersed at different temperatures (283 K, 293 K, 303 K, and 313 K) in a thermostatic bath. The substrates were weighed beforehand. After 2 hours of immersion, the CS samples were removed from the solutions; washed with distilled water, then with acetone; dried; and finally reweighed. Experiments were performed in triplicate for more accuracy to calculate corrosion rates (equation (2) and inhibitory efficiencies (equation (3)) as follows [37]:

$$CR = \frac{w}{A_t}, \quad (2)$$

$$IE\% = \frac{CR_0 - CR}{CR_0} \cdot 100, \quad (3)$$

where CR_0 and CR are the corrosion rates when DCE is absent and present, respectively; A_t is the total surface area of CS samples; w is the mean weight loss; and t is the duration of immersion.

2.7. Electrochemical Measurements. A VoltaLab 40 dynamic potentiostat (PGZ 301) was employed for electrochemical measurements. Tests were performed at 293 K in a thermostatic cell of three electrodes, with a substrate as working electrode, a counter electrode (platinum rod), and a reference electrode ($Hg/Hg_2Cl_2/KCl$ (SCE)). Before each measurement, at open circuit potential (OCP), the working electrode was submerged for one hour in the test solution, and the potential values were taken at stability. For PP, the range of potentials was from −250 mV to +250 mV against the OCP value, with a scan rate of 1 mV·s^{-1}. The following equation gives the inhibitory efficiency percentage (IE%) [18]:

$$IE\% = \frac{i_{0\,corr} - i_{corr}}{i_{0\,corr}} \cdot 100, \quad (4)$$

where $i_{0\,corr}$ and i_{corr} are the densities of corrosion current when DCE is absent and present, respectively.

EIS measurements were accomplished versus OCP with a short amplitude of 10 mV through a frequency range of 100 kHz to 10 mHz. The inhibitory efficiency percentage (IE%) was defined as [19]:

$$IE\% = \frac{R_{ct} - R_{0\,ct}}{R_{ct}} \cdot 100, \quad (5)$$

where R_{ct} and $R_{0\,ct}$ represent the polarization resistance with and without DCE addition, respectively.

2.8. Surface Examination (SEM/EDS). The characteristics of CS sample surface morphology were assessed after soaking for two hours in a 1 M HCl solution, with and without the optimal concentrations of DCE and their NPs using a TESCAN VEGA 3 scanning electron microscope coupled with a BRUKER energy dispersive spectrometer (SEM/EDS).

3. Results and Discussion

3.1. Potentiodynamic Polarization Measurement. Potentiodynamic polarization curves of CS in 1 M HCl solution without and with the addition of different concentrations of DCE and their NPs' optimum concentrations are shown in Figures 1 and 2. These figures demonstrate that the addition of DCE suppresses both cathodic and anodic reactions, and their NPs. The resultant electrochemical parameters including corrosion potential (E_{corr}), corrosion current densities (i_{corr}), inhibitory efficiency percentage (IE%), and the anodic (βa) and cathodic (βc) Tafel slopes (obtained by exploitation of polarization curves) are gathered in Tables 1 and 2. The presence of the studied DCE and their NPs affects the values of both cathodic βc (hydrogen development) and anodic βa (metal dissolution) reactions, suggesting a mixed type of inhibition. Nevertheless, the cathodic part of Tafel slopes seemed to be more affected, which indicates that DCE and their NPs have acted like more cathodic inhibitors [38]. Moreover, the difference in E_{corr} values between the blank and the tested inhibitors is lower than 85 mV, suggesting that the inhibitors exhibit a mixed mode of action [39]. The values of βc and βa did not increase or decrease in a regular manner, confirming the mixed mode of inhibition.

The i_{corr} values decreased with the augmentation of inhibitory concentrations, whereas IE% values increased, denoting that DCE and their NPs have remarkable corrosion inhibitory abilities. It might be due to the adsorption of their organic compounds, thus blocking active sites on the CS surface and consequently slowing down the corrosion process [40].

As shown in Table 2, the maximum inhibitive potency values reached 80.20% with BE at 800 ppm, 72.46% with MDE at 900 ppm, and 58.42% with EAE at 600 ppm. It is to underline that using NPs revealed a better inhibitory effect. They had remarkably increased the inhibitory efficiency (up to 91.20% for the BENPs at 800 ppm, 83.03% for the MDENPs at 900 ppm, and 65.13% for the EAENPs at 600 ppm). Furthermore, it can be observed that the addition of both MDE and their NPs has not caused any change in the anodic and cathodic Tafel slopes, leading to the fact that the inhibitor is first adsorbed onto the steel surface and therefore impedes by simply blocking the reaction sites of the surface.

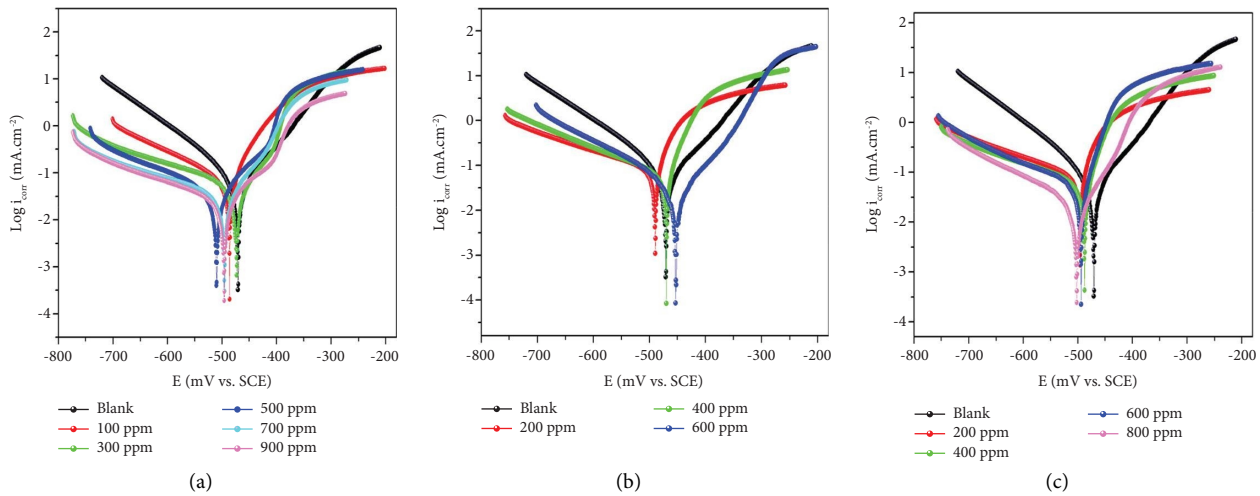

Figure 1: Potentiodynamic polarization curves for CS in 1 M HCl solution without and with different concentrations of (a) MDE, (b) EAE, and (c) BE.

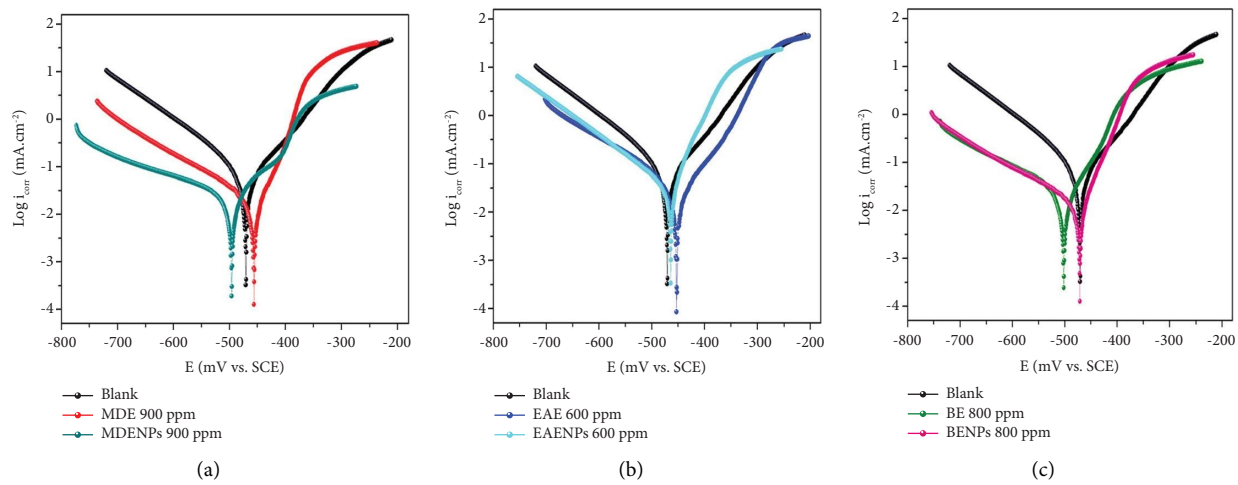

Figure 2: Potentiodynamic polarization curves for CS in 1 M HCl solution without and with optimal concentrations of (a) MDE and its NPs, (b) EAE and its NPs, and (c) BE and its NPs.

Table 1: Polarization parameters and IE% values for CS with various concentrations of DCE at 293 K in a 1 M HCl medium.

Extract	C (ppm)	$-E_{corr}$ (mV/SCE)	i_{corr} (mA·cm^{-2})	β_a (mV·Dec^{-1})	$-\beta_c$ (mV·Dec^{-1})	IE (%)
Blank	0	470.4 ± 1.51	0.0955 ± 1.11	84.1	123.3	—
MDE	100	486.0 ± 0.98	0.0693 ± 1.20	53.7	184.5	27.43
	300	473.1 ± 1.01	0.0563 ± 2.08	38.2	285.6	41.04
	500	509.0 ± 2.21	0.0356 ± 2.75	95.1	207.6	62.27
	700	495.2 ± 1.34	0.0311 ± 1.96	63.1	277.9	67.43
	900	495.8 ± 1.51	0.0263 ± 1.37	114.8	271.8	72.46
EAE	200	489.4 ± 1.76	0.0685 ± 2.11	35.8	232.7	28.27
	400	469.4 ± 2.57	0.0511 ± 1.58	34.2	192.3	46.49
	600	450.7 ± 2.23	0.0397 ± 1.25	64.6	157.3	58.42
BE	200	495.7 ± 1.76	0.0699 ± 1.89	37.5	240.2	26.80
	400	487.6 ± 2.65	0.0536 ± 2.41	35.9	258.1	43.87
	600	494.0 ± 1.87	0.0344 ± 2.12	31.0	178.8	63.97
	800	501.9 ± 2.11	0.0189 ± 1.92	55.0	165.1	80.20

Table 2: Polarization parameters and IE% values for different NPs versus DCE at optimal concentrations at 293 K in a 1 M HCl medium.

C (ppm)	Inhibitor	$-E_{corr}$ (mV/SCE)	i_{corr} (mA·cm^{-2})	β_a (mV·Dec^{-1})	$-\beta_c$ (mV·Dec^{-1})	IE (%)
900	MDE	495.8 ± 1.54	0.0263 ± 1.37	114.8	271.8	72.46
	MDENPS	455.4 ± 0.94	0.0162 ± 1.67	35.5	138.4	83.03
600	EAE	450.7 ± 2.23	0.0397 ± 1.25	64.6	157.3	58.42
	EAENPS	463.9 ± 1.46	0.0333 ± 1.11	43.8	126.7	65.13
800	BE	501.9 ± 2.23	0.0189 ± 1.92	55.0	165.1	80.20
	BENPS	471.0 ± 1.36	0.0085 ± 1.38	38.1	142.4	91.20

3.2. Electrochemical Impedance Spectroscopy. Charge transfer resistance (R_{ct}), CPE parameters (Y_0 and n), double-layer capacitance (C_{dl}), and inhibitory efficiency values are assembled in Tables 3 and 4.

All investigated inhibitors presented a high-frequency capacitive loop with a nonideal semicircle shape due to the metal surface inhomogeneity, which generates a frequency dispersion, and the decomposition of CS is controlled only by charge transfer [41, 42]. The radius of these semicircles gradually augmented, maintaining the same shape along with the concentration increment of DCE and their NPs, indicating the gradual formation of a protective film with the inhibitory molecules [42].

Figures 3 and 4 represent the Nyquist plots for CS in 1 M HCl solution without and with different concentrations of DCE, and their NPs at optimal concentrations at 298 K, respectively.

The experimental EIS data of the DCE and their NPs were fitted to the corresponding equivalent circuit model (ECM), as shown in Figure 5. R_s is the solution resistance, R_{ct} is the charge transfer resistance, and the double-layer capacitance is replaced by a constant phase element (CPE). The following formula expresses CPE impedance [43]:

$$Z_{CPE} = Y_0^{-1}\left(j\omega_{max}\right)^{-n}, \tag{6}$$

where Y_0 is the CPE magnitude, ω_{max} is the angular frequency ($\omega_{max} = 2\pi f_{max}$), f_{max} is the frequency at which the imaginary component of the impedance reaches its maximum values, j is the imaginary root, and n is a deviation parameter of the CPE ($-1 \leq n \leq +1$). CPE behaves as a resistor, an inductor, and a capacitor when $n = 0, -1$, and $+1$, respectively [44]. The double-layer capacitance (C_{dl}) was obtained by the following formula [43]:

$$C_{dl} = Y_0\left(j\omega_{max}\right)^{n-1}. \tag{7}$$

From Tables 3 and 4, the obtained values of C_{dl} decreased conversely with the inhibitory concentrations, which denotes that the inhibitors' adsorption on the metal surface has enhanced, and this may be ascribed to the electrical double-layer growth [45]. R_{ct} values were increased with the inhibitory concentration, and the registered IE% values were 78.97% with BE at 800 ppm, 70.79% with MDE at 900 ppm, and 60.27% with EAE at 600 ppm. Moreover, in the case of using NPs, efficiency values remarkably rose to 89.22% for BENPs at 800 ppm, 78.98% at 900 ppm for MDENPs, and 68.38% at 600 ppm for EAENPs, which confirms the reliability of the obtained PP measurements.

3.3. Weight Loss Measurements. This procedure was employed to evaluate the inhibitory effect of different DCE concentrations on CS samples in 1 M HCl for 2 hours at different temperatures (283, 293, 303, and 313 K). The obtained values of corrosion rates (CR) and inhibitory efficiency percentage (IE%) are listed in Table 5. The examination of Figure 6 shows that the CR decreased with the increase in DCE concentrations and ascended along with temperature elevation, which implies a decrease in IE% as exhibited in Figure 7. At 293 K, the BE has the higher IE% value of 80.38% at 800 ppm, while the MDE and EAE values are 72.23% and 52.33% at 900 ppm and 600 ppm, respectively. The inhibitive effect of DCE against the dissolution of CS is possibly a result of their molecules being present in the medium, which use adsorption phenomena to form a barrier of protection on the surface of CS [19, 46].

3.4. Adsorption Isotherm. For a better understanding of the inhibitory mechanism on the CS surface, adsorption isotherm models such as Freundlich, Temkin, Langmuir, and Frumkin were tested. The results are summarized in Table 6. The choice of adsorption isotherm was based on the closeness of correlation coefficient (r^2) values to 1 at all tested temperatures (283–313 K), and the Freundlich model provided the best fit.

The Freundlich adsorption isotherm was calculated using the following equation [47]:

$$\log\theta = \log K_{Ads} + n\log C, \tag{8}$$

where C is the inhibitory concentration, θ is the surface coverage, and K is the adsorption constant. Figure 8 shows the straight lines of $\log\theta/\log C$ for DCE at different temperatures.

K_{Ads} values reported in Table 7 are determined from the intercepts of the curves from Figure 8. As the temperature increased, K_{Ads} values decreased, probably owing to the desorption of DCE components previously adsorbed on the surface of metal [48].

3.5. Thermodynamic Parameters. The standard adsorption-free enthalpy ΔG°_{ads} can be calculated as follows [49]:

$$\Delta G^{\circ}_{ads} = -\mathrm{RTln}\left(C_{H_2O}\cdot K_{ads}\right), \tag{9}$$

where R is the gas constant, T is the absolute temperature, and C_{H_2O} is the concentration of water expressed in mg·L^{-1} with an estimated value of 10^6.

Table 3: Impedance parameters and IE% values for CS with various concentrations of DCE at 293 K in a 1 M HCl medium.

Extract	C (ppm)	R_{ct} ($\Omega\cdot cm^2$)	$Y_0.10^{-6}(S^n\cdot\Omega^{-1}\cdot cm^{-2})$	n	C_{dl} ($\mu F\cdot cm^{-2}$)	IE (%)
Blank	0	251.4 ± 1.02	81.28 ± 1.10	0.68 ± 2.00	63.30	—
MDE	100	348.7 ± 0.84	22.77 ± 1.00	0.40 ± 1.32	144.2	27.90
	300	390.8 ± 0.53	20.87 ± 0.82	0.85 ± 1.81	101.8	35.67
	500	568.2 ± 1.30	37.05 ± 2.01	0.51 ± 1.99	44.25	55.75
	700	735.8 ± 1.90	16.18 ± 1.72	0.34 ± 1.52	27.25	65.83
	900	860.7 ± 0.74	21.02 ± 1.54	0.39 ± 1.38	23.29	70.79
EAE	200	349.3 ± 0.67	35.34 ± 1.52	0.53 ± 0.82	45.55	28.02
	400	447.8 ± 1.22	49.56 ± 1.61	0.63 ± 1.05	28.17	43.85
	600	632.6 ± 1.09	25.07 ± 1.38	0.45 ± 1.43	14.21	60.27
BE	200	361.0 ± 1.93	10.81 ± 1.90	0.27 ± 1.18	139.2	30.51
	400	574.5 ± 1.01	13.70 ± 1.43	0.31 ± 1.65	87.53	56.20
	600	729.8 ± 0.83	21.04 ± 1.24	0.39 ± 1.28	54.51	65.52
	800	1188.0 ± 0.10	31.66 ± 1.81	0.47 ± 1.11	26.78	78.87

Table 4: Impedance parameters and IE% values for CS in 1 M HCl solution containing different NPs versus DCE at optimal concentrations at 293 K.

C (ppm)	Inhibitor	R_{ct} ($\Omega\cdot cm^2$)	$Y_0.10^{-6}(S^n\cdot\Omega^{-1}\cdot cm^{-2})$	n	C_{dl} ($\mu F\cdot cm^{-2}$)	IE (%)
900	MDE	860.7 ± 0.74	21.02 ± 1.54	0.39 ± 1.38	23.29	70.79
	MDENPS	1196.2 ± 0.74	40.97 ± 1.02	0.54 ± 1.02	16.75	78.98
600	EAE	632.6 ± 1.09	25.07 ± 1.38	0.45 ± 1.43	14.21	60.27
	EAENPS	777.9 ± 2.02	65.04 ± 1.02	0.72 ± 1.02	5.11	68.38
800	BE	1188.0 ± 0.10	31.66 ± 1.81	0.47 ± 1.11	26.78	78.87
	BENPS	2329.1 ± 0.10	38.85 ± 1.02	0.53 ± 1.02	18.68	89.22

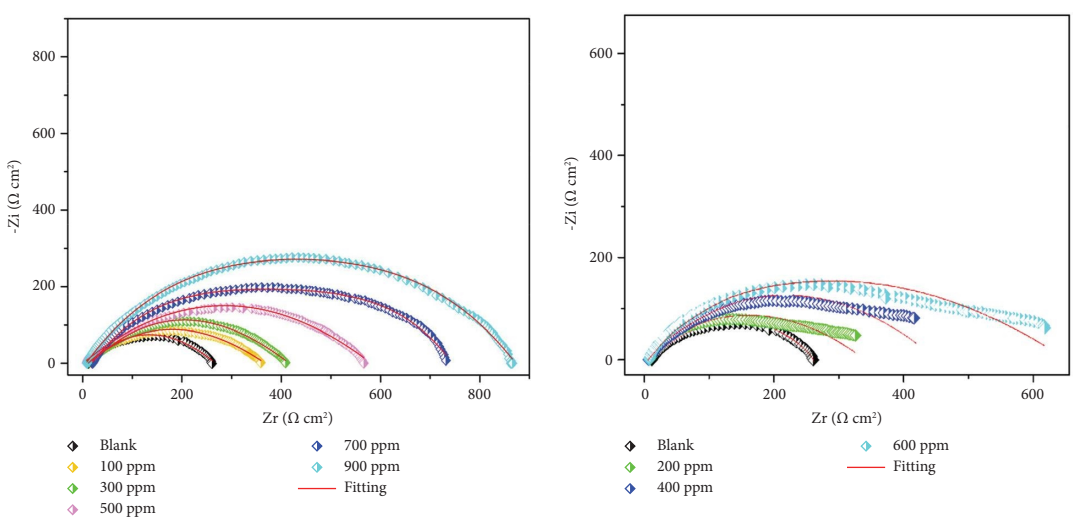

Figure 3: Continued.

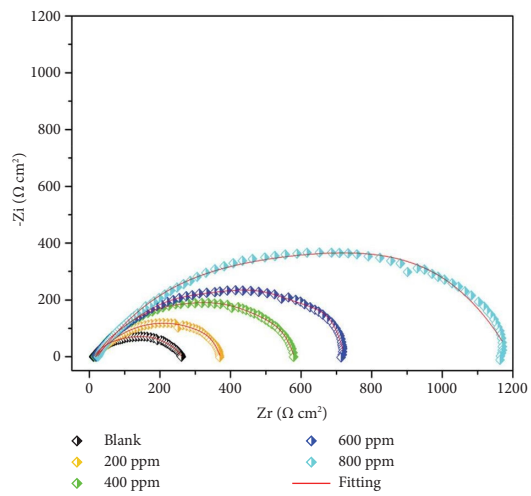

(c)

Figure 3: Fitted Nyquist representation for 1 M HCl with and without (a) MDE, (b) EAE, and (c) BE.

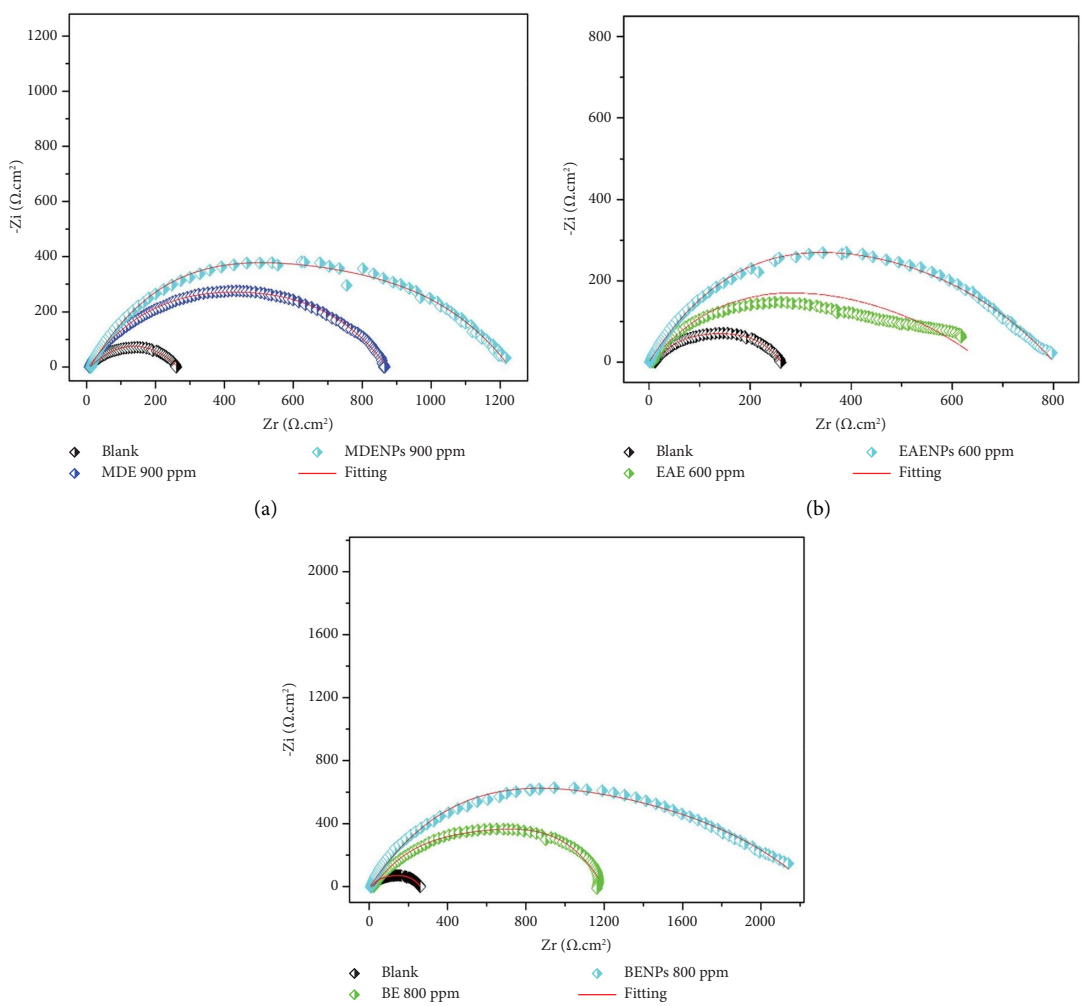

Figure 4: Fitted Nyquist representation for 1 M HCl with and without (a) MDENPs, (b) EAENPs, and (c) BENPs at optimal concentrations.

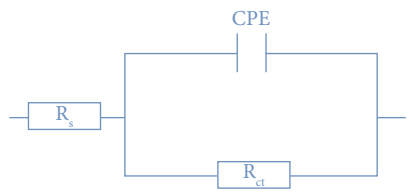

Figure 5: ECM used for the simulation of impedance data for both DCE and NPs.

Table 5: CR and IE% values from WL tests using different concentrations of DCE for CS in HCl (1 M) solution at various temperatures.

	C (ppm)	283 K		293 K		303 K		313 K	
		CR ($mg{\cdot}cm^{-2}{\cdot}h^{-1}$)	IE (%)	CR ($mg{\cdot}cm^{-2}{\cdot}h^{-1}$)	IE (%)	CR ($mg{\cdot}cm^{-2}{\cdot}h^{-1}$)	IE (%)	CR ($mg{\cdot}cm^{-2}{\cdot}h^{-1}$)	IE (%)
MDE	Blank	0.1498 ± 0.02	—	0.1790 ± 0.02	—	0.2060 ± 0.02	—	0.2306 ± 0.03	—
	100	0.0914 ± 0.03	22.71	0.1165 ± 0.02	21.24	0.1483 ± 0.01	18.98	0.1718 ± 0.03	17.24
	300	0.0796 ± 0.03	32.69	0.1019 ± 0.01	31.06	0.1326 ± 0.03	27.58	0.1560 ± 0.02	24.84
	500	0.0622 ± 0.01	47.34	0.0799 ± 0.03	45.97	0.1098 ± 0.02	39.99	0.1398 ± 0.02	32.62
	700	0.0483 ± 0.02	59.11	0.0639 ± 0.03	56.80	0.0879 ± 0.03	50.88	0.1129 ± 0.03	47.04
	900	0.0299 ± 0.01	74.69	0.0410 ± 0.02	72.23	0.0616 ± 0.02	66.35	0.0821 ± 0.02	60.43
EAE	200	0.0874 ± 0.02	36.96	0.1155 ± 0.01	28.57	0.1534 ± 0.02	23.92	0.2221 ± 0.03	19.91
	400	0.0733 ± 0.03	47.10	0.0938 ± 0.02	41.58	0.1304 ± 0.03	34.9	0.1925 ± 0.02	30.60
	600	0.0550 ± 0.04	60.30	0.0771 ± 0.03	52.33	0.1086 ± 0.03	45.78	0.1687 ± 0.01	39.18
BE	200	0.1013 ± 0.02	50.01	0.1427 ± 0.03	41.80	0.1930 ± 0.02	38.98	0.2740 ± 0.03	26.03
	400	0.0872 ± 0.02	56.97	0.1173 ± 0.03	47.84	0.1654 ± 0.03	44.45	0.2421 ± 0.02	34.63
	600	0.0639 ± 0.01	68.46	0.0969 ± 0.02	62.67	0.1321 ± 0.02	58.25	0.2039 ± 0.02	44.95
	800	0.0460 ± 0.02	81.85	0.0713 ± 0.02	80.38	0.1121 ± 0.02	71.02	0.1727 ± 0.02	53.37

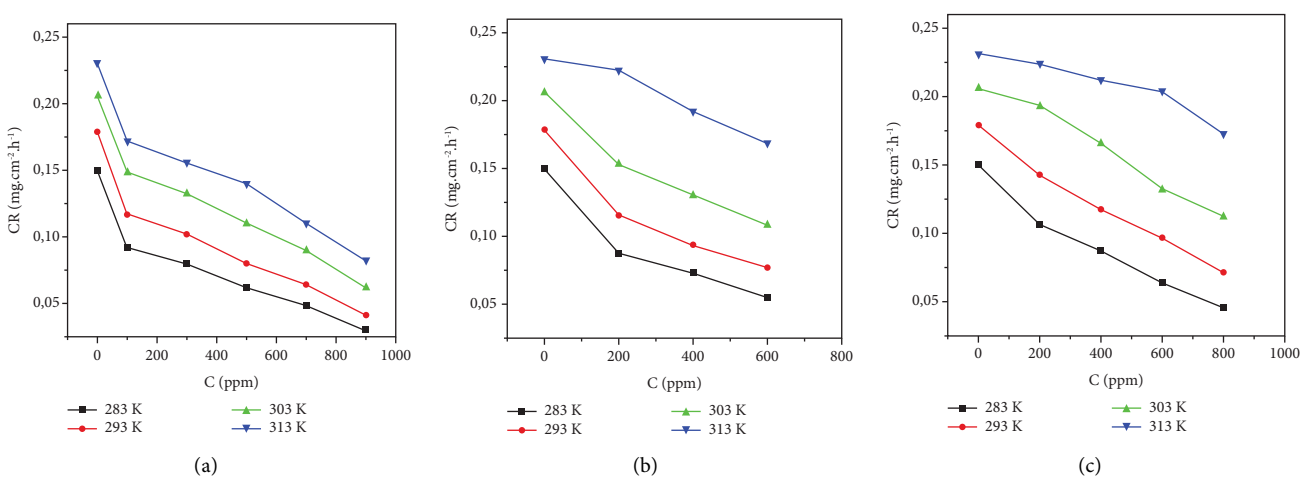

Figure 6: Corrosion rate and concentration variation relationship of CS for: (a) MDE, (b) EAE, and (c) BE in a 1 M HCl solution.

The standard adsorption enthalpy (ΔH°_{ads}) can be calculated using the Van 't Hoff equation as follows [50]:

$$\frac{\delta \ln K_{ads}}{\delta T} = \frac{\Delta H^{\circ}_{ads}}{RT^2}. \quad (10)$$

The equation is rewritten as follows:

$$\ln K_{ads} = \frac{-\Delta H^{\circ}_{ads}}{RT} + I, \quad (11)$$

where I is the integration constant.

Figure 9 demonstrates the linear regression of $\ln K_{ads}$ against $1/T$.

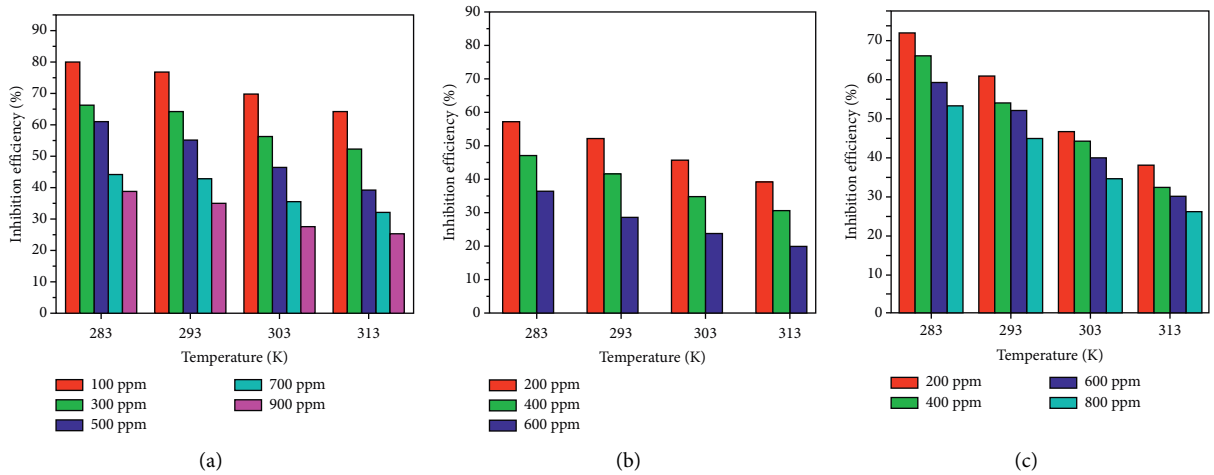

Figure 7: Temperature and concentrations impact on IE% of CS for: (a) MDE, (b) EAE, and (c) BE in HCl (1 M) solution.

Table 6: Correlation coefficients of the different adsorption isotherms.

Extract	Temperature (K)	Correlation coefficient (r^2)			
		Freundlich	Temkin	Langmuir	Frumkin
MDE	283	0.9287	0.9012	0.8287	0.9178
	293	0.9355	0.8355	0.9201	0.8901
	303	0.9298	0.9298	0.9086	0.8086
	313	0.8999	0.8365	0.9049	0.9384
EAE	283	0.9948	0.8556	0.9341	0.9341
	293	0.9998	0.8927	0.9383	0.9383
	303	0.9969	0.8478	0.9597	0.8897
	313	0.9999	0.7493	0.8307	0.8307
BE	283	0.9637	0.8724	0.9334	0.8453
	293	0.9920	0.9076	0.9440	0.9092
	303	0.9911	0.9201	0.9242	0.9245
	313	0.9877	0.9241	0.9162	0.9112

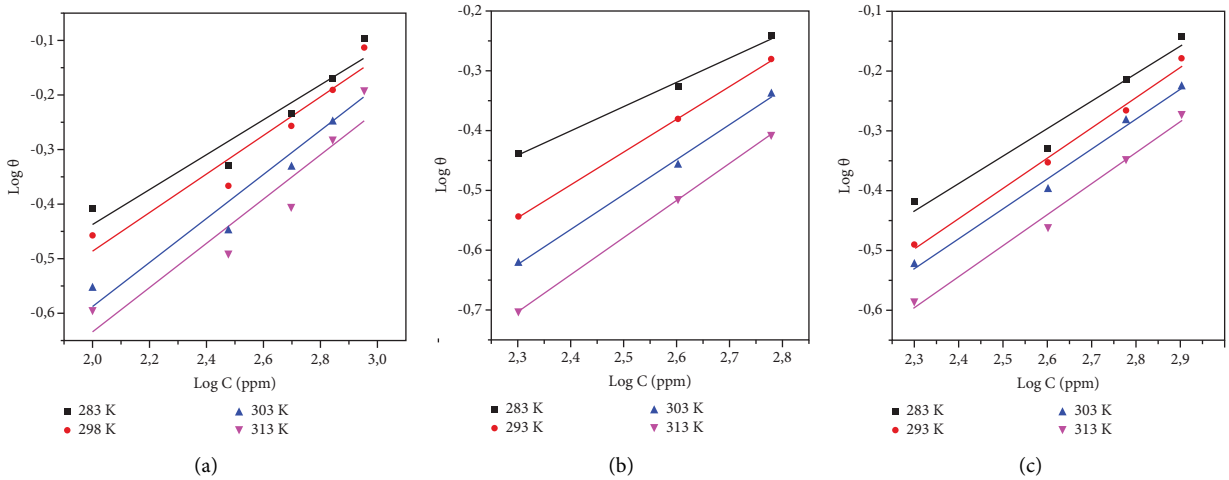

Figure 8: Freundlich isotherm adsorption at various temperatures for: (a) MDE, (b) EAE, and (c) BE.

Table 7: Standard thermodynamic parameters of the adsorption of MDE, EAE, and BE in a 1 M HCl solution.

Extract	T (K)	k_{ads} (L mg^{-1})	ΔG°_{ads} (kJmol^{-1})	ΔH°_{ads} (kJmol^{-1})	ΔS°_{ads} (Jmol^{-1}K^{-1})
MDE	283	0.084922	−26.70	−22.22	−15.83
	293	0.065223	−27.00		−16.31
	303	0.040417	−26.72		−14.85
	313	0.036523	−27.33		−16.32
EAE	283	0.041697	−25.03	−4.68	−55.30
	293	0.015487	−23.50		−58.63
	303	0.010646	−23.35		−57.19
	313	0.007595	−23.25		−55.68
BE	283	0.032259	−24.42	−15.51	−31.48
	293	0.021909	−24.34		−30.13
	303	0.020830	−25.05		−31.48
	313	0.016301	−25.23		−31.05

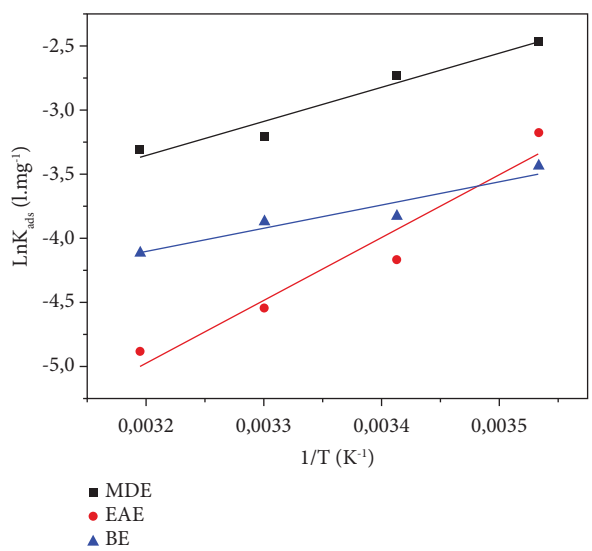

Figure 9: Straight lines of ln K_{ads} versus $1/T$ of MDE, EAE, and BE at different temperatures.

ΔH°_{ads} value was calculated from the slope $(-\Delta H^{\circ}_{ads}/R)$ and listed in Table 7. From the obtained results of ΔG°_{ads} and ΔH°_{ads}, the standard adsorption entropy (ΔS°_{ads}) is determined by the Gibbs–Helmholtz relation [51]:

$$\Delta S^{\circ}_{ads} = \frac{\Delta H^{\circ}_{ads} - \Delta G^{\circ}_{ads}}{T}. \quad (12)$$

From the above table, the spontaneity of the adsorption process was pointed out by the negative values of ΔG°_{ads}. The calculated values of the adsorption-free enthalpy are less than -20 kJmol^{-1}, which indicates a physical adsorption mechanism [52]. The negative values of ΔH°_{ads} show that inhibitory adsorption is an exothermic process [53]. Additionally, the negative sign of ΔS°_{ads} suggests that the decrease in disorder is due to the adsorption process, attributable to the adsorption of the inhibitor on the surface of steel [54].

3.6. Activation Parameters for Corrosion Reaction. The corrosion reaction can be regarded as an Arrhenius-type process, allowing for the calculation of activation parameters using the following equation [55]:

$$\ln C_R = -\frac{E_a}{RT} + \ln \mathrm{Ds}, \quad (13)$$

where E_a is the apparent activation energy of the CS corrosion, R is the universal gas constant, T is the absolute temperature, and Ds is the Arrhenius pre-exponential factor.

The activation energies (E_a) listed in Table 8 were derived by analyzing the slopes of the $\ln C_R$ versus $1/T$ plots (Figure 9).

The examination of Table 8 shows that in the presence of the DCE, the E_a values were higher than those in their absence, indicating that the adsorption process on the substrates follows a physisorption mode [19, 56, 57].

The determination of the activation entropy and enthalpy $(\Delta S_a$ and $\Delta H_a)$ can be obtained by the Arrhenius transition state equation (55):

$$\ln \frac{C_R}{T} = \left[\ln \frac{R}{hN_a} + \frac{\Delta S_a}{R}\right] - \frac{\Delta H_a}{RT}, \quad (14)$$

where h is Planck's constant and N_a is Avogadro's number.

The values of ΔH_a and ΔS_a listed in Table 8 were extracted from the straight line given by the plot of $\ln C_R/T$ vs. $1/T$ (Figure 10), with $-\Delta H_a/R$ as a slope and $\ln R/hN_a + \Delta S_a/R$ as an intercept. Arrhenius plots of ln (CR/T) versus 1/T for CS corrosion in a 1 M HCl of the extracts are provided in Figure 11. The positive ΔH_a values suggest that the decomposition process of CS was endothermic [58]. The negative values of ΔS_a suggest that the activated complex primarily involves association instead of dissociation, which implies that an augmentation in randomness was observed during the association of reactants to an activated complex [19, 59, 60].

3.7. Colorimetric Evaluation of Corrosion Products. The optical evaluation of corrosive solutions was accomplished using UV-vis spectroscopy. The tracking of ferrous iron ions and phenolic contents was made for the blank and optimal concentrations before and after corrosion tests.

3.7.1. Phenolic Content Evolution. The quantitative evaluation of corrosion test solutions showed that the phenolic content decreased after 2 hours of immersion

Table 8: Activation parameters of different DCE concentrations for CS in a 1 M HCl.

Extract	C (ppm)	E_a (kJ·mol^{-1})	ΔH_a (kJ·mol^{-1})	$10^{-1}\Delta S_a$ (J·mol^{-1}·K^{-1})
Blank	0	10.59	8.11	−231.46
MDE	100	15.75	13.28	−217.32
	300	16.82	14.35	−214.71
	500	20.20	17.73	−204.98
	700	21.08	18.61	−203.93
	900	25.28	22.81	−193.14
EAE	200	22.63	20.15	−193.72
	400	23.64	21.17	−191.97
	600	27.18	24.71	−181.49
BE	200	19.84	17.36	−201.85
	400	22.18	19.71	−195.13
	600	27.88	25.71	−177.56
	800	32.55	30.08	−163.87

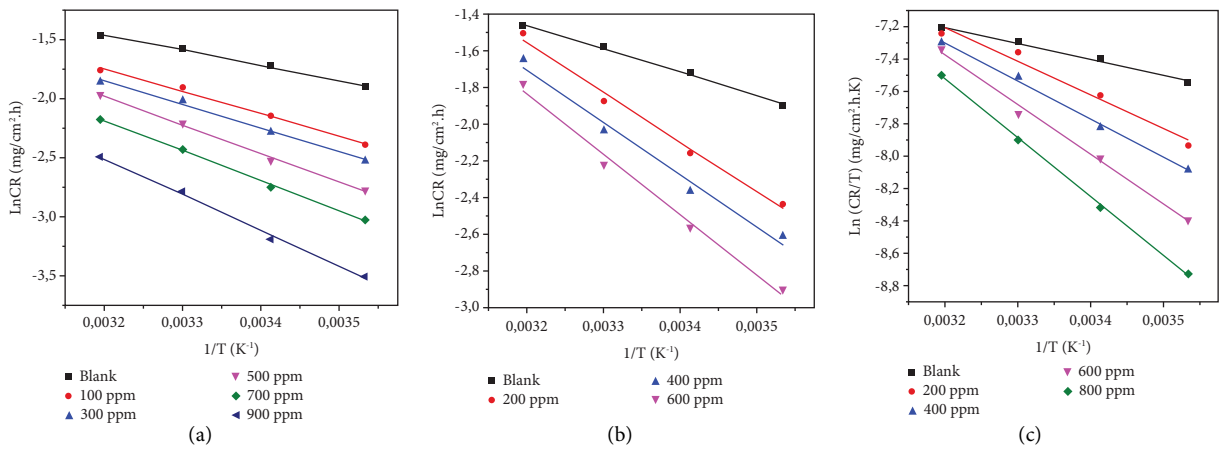

Figure 10: Arrhenius plots of $\ln C_R$ versus $1/T$ for the CS corrosion in a 1 M HCl of: (a) MDE, (b) EAE, and (c) BE.

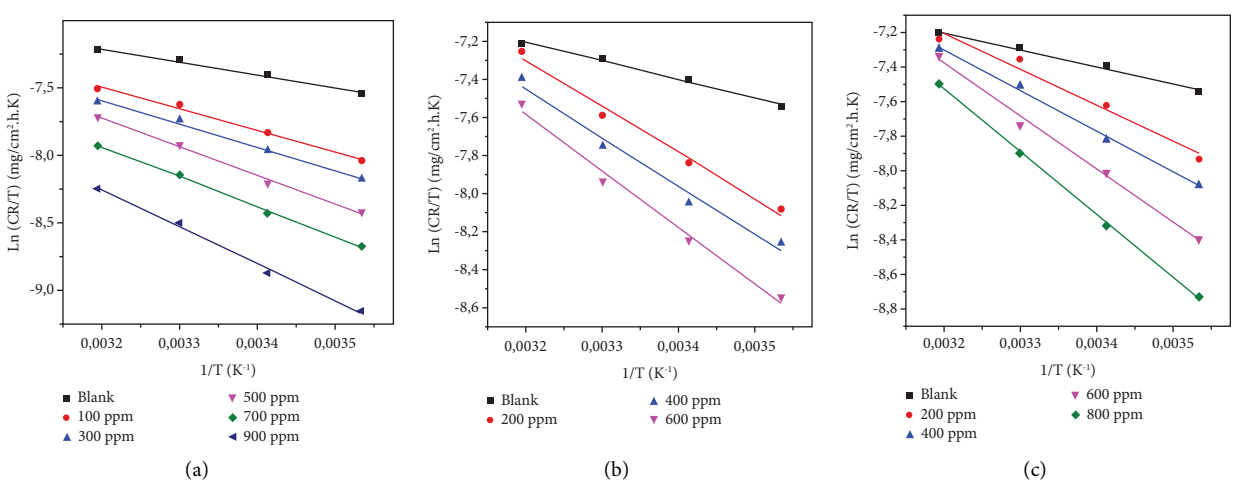

Figure 11: Arrhenius plots of ln (CR/T) versus 1/T for CS corrosion in a 1 M HCl of: (a) MDE, (b) EAE, and (c) BE.

in the aggressive solution (Table 9), proving the consumption of phenolics through adsorption on the steel surface, which confirms the results mentioned above. The measurements are taken according to the calibration curve prepared from gallic acid ($y = 0.0034x + 0.1044$, $R^2 = 0.997$).

Table 9: Total phenolic content (μg·GAE/mg) of corrosion test solutions before and after immersion.

Extracts	Before	After
MDE	128.51 ± 3.86	64.23 ± 1.62
EAE	44.12 ± 2.99	28.65 ± 2.11
BE	142.91 ± 1.54	85.13 ± 1.94

3.7.2. Ferrous Ion Determination. According to the calibration curve made from iron solution ($y = 16.415x + 0.0906$, $R^2 = 0.999$), the iron ion amounts in test solutions containing DCE decreased compared with the blank, confirming the corrosion inhibition. However, and remarkably, these quantities decreased much more in the presence of their NPs. It is to highlight that the inhibitory efficiency increased with a decrease in Fe^{2+} concentration when adding DCE and increased even more when their NPs were added (Table 10), which is confirmed by the solution color change. It is worth noting that BE was the most effective inhibitor, followed by MDE and EAE, respectively. Nevertheless, the use of NPs showed an extra decrease of 104 ppm for MDENPs, 79.104 ppm for EAENPs, and 112 ppm for BENPs. There is a harmony between the decrease in iron quantities, the DCE inhibitory power, and their NPs against corrosion.

3.7.3. UV-Visible Spectral Analysis. The UV-visible spectroscopic assessment was employed to validate the ZnO-NPs generation. Figure 12 depicts the absorption plots of ZnO-NPs eco-friendly prepared from extracts of *Daucus crinitus*. It is widely recognized that UV-vis plots are frequently utilized to assess the size and shape of nanoparticles in a water-based suspension [61, 62]. Zinc oxide nanoparticles usually exhibit a prominent UV absorption peak in their UV-vis spectra, with a maximum observed at approximately 370–380 nm as a result of the bandgap absorption of the nanoparticles. As seen in Figure 12, all formed ZnO-NPs (MDENPs, EAENPs, and BENPs) exhibited strong UV absorption spectra with characteristic absorption peak at about 375 nm. The UV-vis spectra of ZnO nanoparticles usually indicate characteristic peak at 375 nm [63]. It is also evident that significant sharp absorption of ZnO indicates the monodispersed nature of the nanoparticle distribution. The absorption peak centered at about 378 nm is the characteristic peak for hexagonal wurtzite ZnO nanoparticles.

3.8. Surface Examination (SEM-EDS). To examine the CS surface morphology, the samples were immersed for 2 hours at 298 K in a 1 M HCl solution with and without the addition of the optimal concentration of DCE and their NPs. The inspection of Figure 13 shows that the treated surface with 1 M HCl was deeply cracked and pitted compared with the solutions containing inhibitors (Figures 14–19), which is smoother thanks to the organic molecules provided by the inhibitors adsorbed on the CS surface, creating a protective layer. In the presence of 600 ppm of EAE, the surface had fewer holes and ravines, as seen in Figure 14. However, from Figure 13, the presence of 900 ppm of MDE reduces the CS surface damage, and better results with 800 ppm of BE are observed in Figure 15. Additionally, the results with NPs were better in terms of surface homogeneity and efficiencies in the same order as DCE. Amazingly, the best surface morphologies were observed in the presence of 800 ppm of BENPs, followed by 900 ppm of MDENPs, and then 600 ppm of EAENPs, as shown in Figures 17–19, respectively. It is intended to highlight that the spherical shape of NPs confirms their successful synthesis. The EDS analysis revealed the presence of Fe, C, O, Cl, and Zn (Figures 13–19 and Table 11). The uninhibited sample surface composition showed the wt% of Fe (93.14%), C (2.03%), O (1.61%), and Cl (3.22%). It should be noted that the decrease in the Fe percentage in SEM/EDS analysis when inhibitors are present compared to their absence is due to the adsorption behavior of inhibitory molecules on the Fe surface. When inhibitors are present, they interact with Fe atoms, forming a protective layer that inhibits corrosion. This interaction reduces the exposure of Fe atoms to corrosive agents, resulting in a lower Fe percentage detected through SEM/EDS analysis [64–67]. Moreover, the oxygen wt% increased for BE (5.83%)-BENPs (5.95%), MDE (3.86%)-MDENPs (4.33%), and EAE (2.61%)-EAENPs (3.52%), suggesting a difference in oxygen atoms in the inhibitor's composition. It is also to

Table 10: Concentrations of generated Fe^{2+} in test solutions without and with DCE and their NPs.

Solution	$C_{Fe^{2+}}.10^4$ (ppm)
HCl	939 ± 2.86
HCl + MDE	676 ± 1.63
HCl + MDENPs	572 ± 2.91
HCl + EAE	479 ± 1.12
HCl + EAENPs	400 ± 2.06
HCl + BE	416 ± 0.98
HCl + BENPs	304 ± 1.74

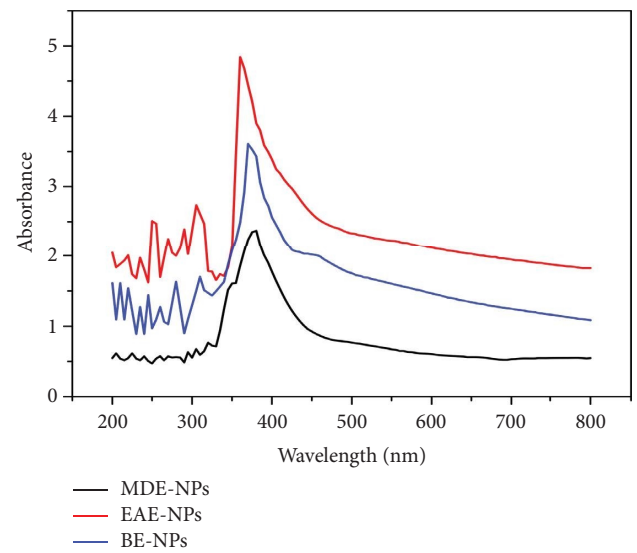

Figure 12: UV-vis spectra of ZnO-NPs biosynthesized using *Daucus crinitus* extracts.

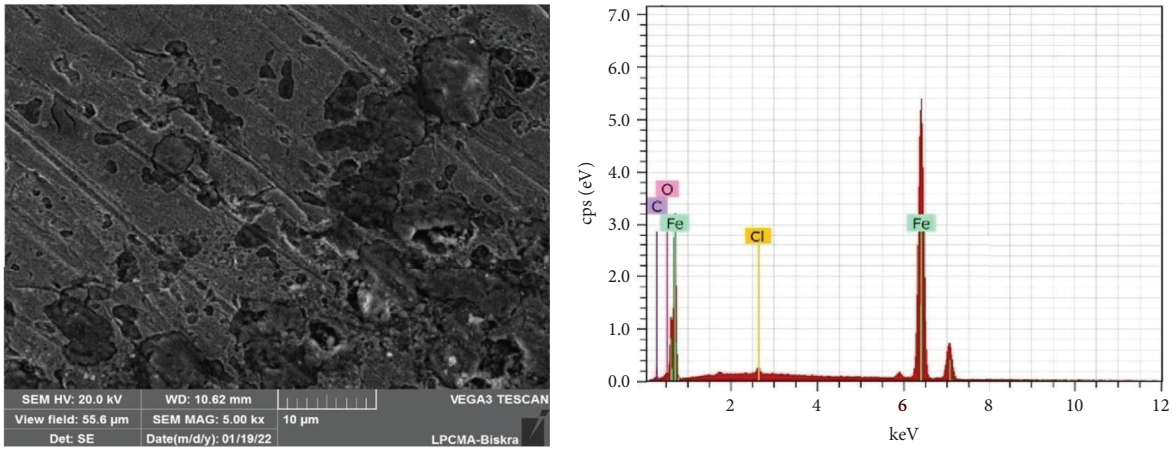

Figure 13: SEM image and EDS analysis of X60 after immersion in a 1 M HCl.

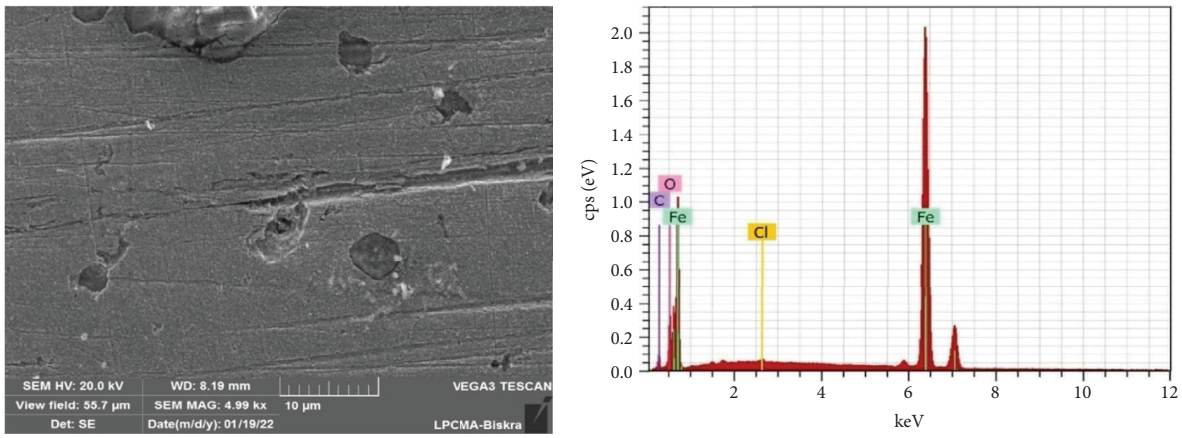

Figure 14: SEM image and EDS analysis of X60 CS immersed in a 1 M HCl with 900 ppm of MDE.

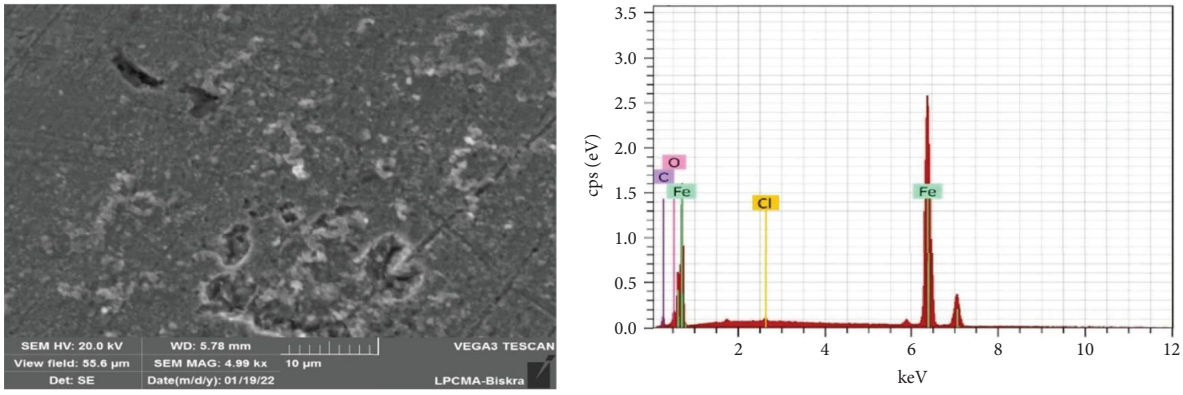

Figure 15: SEM image and EDS analysis of X60 CS immersed in a 1 M HCl with 600 ppm of EAE.

highlight that a new peak of the Zn atom appeared in the spectra of the samples covered with nanoparticles because of the zinc oxide agglomeration with the organic molecules. Additionally, the carbon %wt increased for all extracts when the inhibitors were added, whereas this quantity decreased in the nanoparticles due to the covering of the organic molecules by the ZnO, which is confirmed by the SEM images. Once more, when the inhibitors are added, the Cl wt% decreases, denoting that the studied inhibitors prevent further attacks of the corrosive chloride ions [64]. Moreover, and remarkably, an extra reduction in chloride amounts was observed in the case of using NPs, accompanied by an enhancement of surface homogeneity, thus indicating their ability to cover more areas and provide more protection from the corrosive medium.

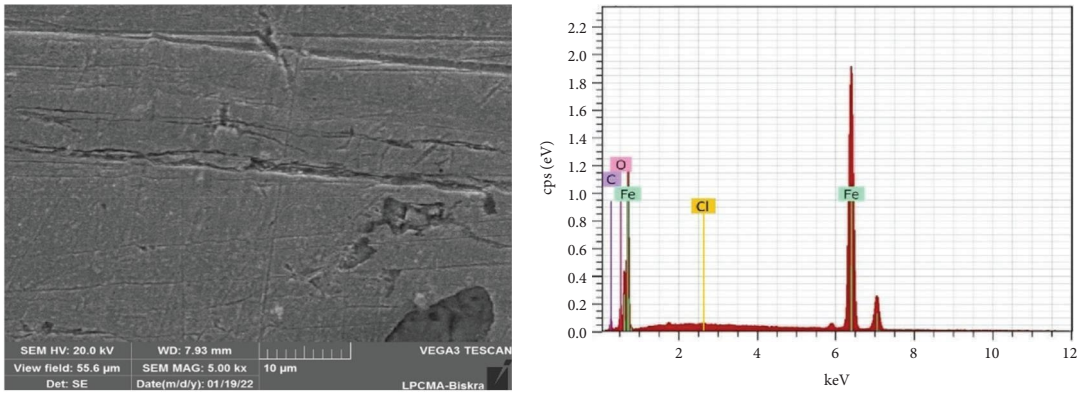

Figure 16: SEM image and EDS analysis of X60 CS immersed in a 1 M HCl with 800 ppm of BE.

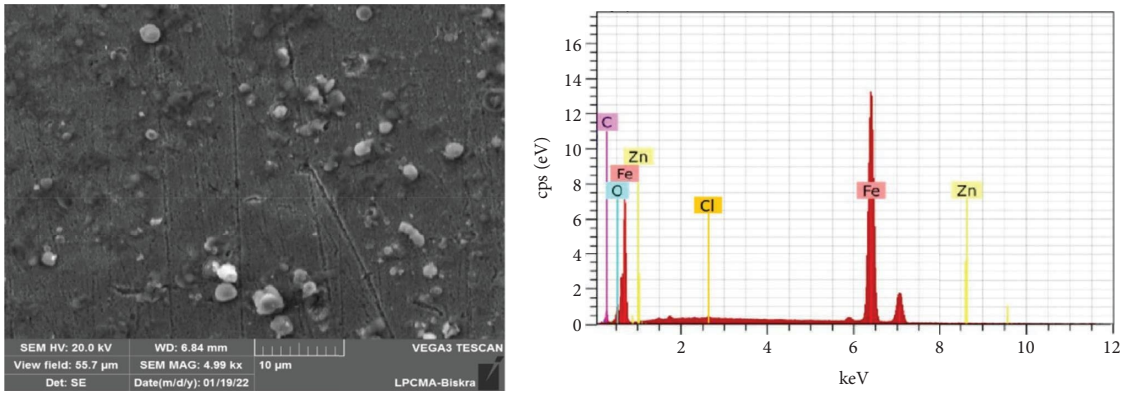

Figure 17: SEM image and EDS analysis of X60 CS immersed in a 1 M HCl with 900 ppm of MDENPs.

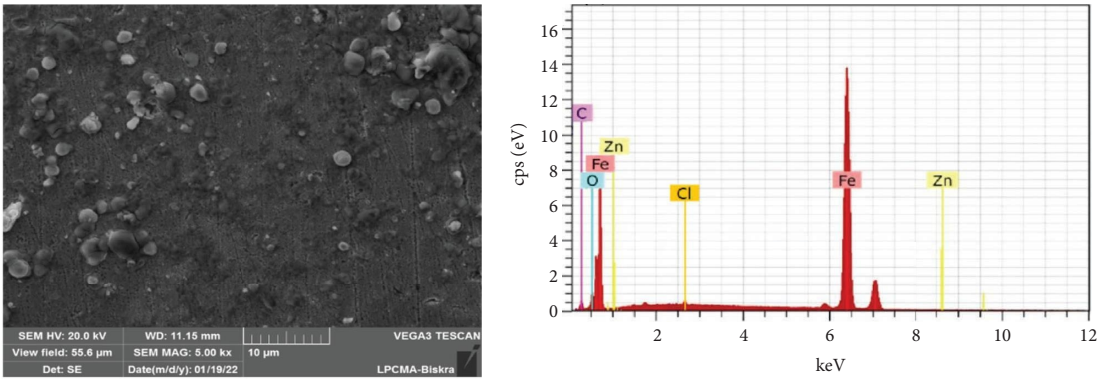

Figure 18: SEM image and EDS analysis of X60 CS immersed in a 1 M HCl with 600 ppm of EAENPs.

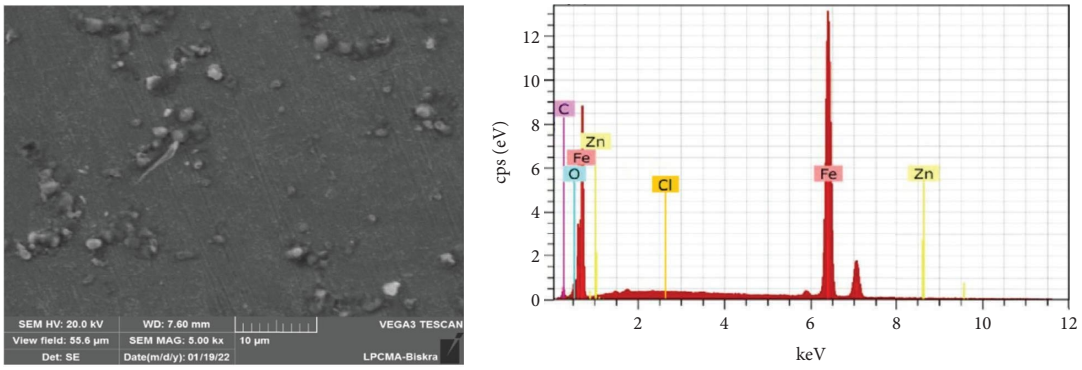

Figure 19: SEM image and EDS analysis of X60 CS immersed in a 1 M HCl with 800 ppm of BENPs.

Table 11: EDS parameters of the X60 CS surface without and with the addition of DCE and their NPs.

Medium	Element	Series	Norm. C (wt.%)	Atom. C (at.%)	Error (wt.%)
HCl	Fe	K	93.14	72.45	2.31
	C	K	2.03	13.91	1.22
	O	K	1.61	3.78	0.49
	Cl	K	3.22	9.86	1.10
		Total:	100	100	
HCl + MDE	Fe	K	89.17	67.21	2.09
	C	K	6.08	21.33	1.53
	O	K	3.86	9.42	0.57
	Cl	K	0.89	2.04	0.34
		Total:	100	100	
HCl + EAE	Fe	K	90.34	70.05	2.17
	C	K	6.04	20.16	1.33
	O	K	2.61	7.15	0.51
	Cl	K	1.01	2.64	0.50
		Total:	100	100	
HCl + BE	Fe	K	86.64	63.92	2.25
	C	K	6.78	22.25	0.97
	O	K	5.83	11.86	1.19
	Cl	K	0.75	1.97	0.44
		Total:	100	100	
HCL + MDENPs	Fe	K	88.78	70.05	2.38
	C	K	5.84	19.16	1.19
	O	K	4.33	8.13	0.56
	Cl	K	0.76	1.84	0.42
	Zn	K	0.29	0.82	0.03
		Total:	100	100	
HCl + EAENPs	Fe	K	90.03	70.16	2.23
	C	K	5.30	19.56	1.15
	O	K	3.52	7.28	0.47
	Cl	K	0.93	2.24	0.15
	Zn	K	0.22	0.76	0.08
		Total:	100	100	
HCl + BENPs	Fe	K	86.16	65.74	2.27
	C	K	6.91	22.86	1.30
	O	K	5.95	8.89	0.60
	Cl	K	0.67	1.66	0.34
	Zn	K	0.31	0.85	0.12
		Total:	100	100	

Table 12: Corrosion inhibitory efficiency of some plant extracts.

Plant extract	Inhibition efficiency (%)	Concentration (ppm)	Reference
Daucus crinitus	91.20	800	Present work
Thunbergia fragrans	81.00	500	[6]
Lamium flexuosum	83.50	900	[7]
Taxus baccata	82.00	800	[5]
Uncaria gambir	95.00	1000	[8]
Dacryodes edulis	79.00	800	[9]
Hibiscus sabdariffa	91.00	500	[10]
Rosa canina	86.00	800	[11]
Solanum melongena	70.00	500	[12]
Lawsonia inermis	92.60	1200	[68]
Dendrocalamus sinicus	79.20	200	[69]
Jasmine nudiflorum	93.10	1000	[70]
Salvia officinalis	72.50	500	[71]
Strictosamide from *Uncaria laevigata*	92.00	160	[72]
Punica granatum	86.90	1000	[73]

Table 12: Continued.

Plant extract	Inhibition efficiency (%)	Concentration (ppm)	Reference
Valeriana wallichii	91.45	500	[74]
Alkanna tinctoria	90.46	500	[75]
Feverfew (*Tanacetum parthenium*)	98.10	400	[76]
Curcumin	82,72	500	[77]
Parsley	84.76	500	[77]
Cassia bark	88.02	500	[77]
Rosa damascene	75.00	300	[78]
Asphodelus ramosus	89.81	700	[79]
Scorzonera undulata	83.00	400	[80]

There has been a growing interest in recent years to explore plant extracts as eco-friendly corrosion inhibitors, owing to their abundant availability and low environmental impact. The table below provides the inhibitory efficiency derived from various studies that have investigated the use of plant extracts to inhibit corrosion. Notably, the results found in the current study compared to the results of corrosion inhibition by other plant extracts as shown in Table 12 indicate that DCE exhibits particularly promising inhibitory efficiency, which reached 80.20% in the presence of 800 ppm. Furthermore, this efficiency was improved when ZnO-NPs were synthesized using DCE as an inhibitor, reaching an efficiency of 91.20%.

4. Conclusion

The study investigates the use of *Daucus crinitus* extracts (DCE) and eco-friendly synthesized ZnO nanoparticles (NPs) to inhibit the corrosion of API 5L-X60 carbon steel in a 1 M HCl corrosive environment. Through a comprehensive analysis utilizing techniques such as WL, EIS, and PP measurements, coupled with spectroscopic and surface (SEM-EDS) characterization, several significant findings were elucidated. Notably, the successful synthesis of zinc oxide nanoparticles using DCE via a green approach was confirmed. The investigation revealed that both DCE and their NPs exhibit notable inhibitory effects on carbon steel in 1 M HCl medium. Particularly, the introduction of DCE-derived NPs significantly enhanced the inhibitory efficiency percentage (IE%) from 80.20% to 91.20% at 298 K with 800 ppm of DCE. Increasing the inhibitory concentration resulted in higher inhibitory efficiencies, while increasing temperature lowered it. Physical adsorption of inhibitors onto the carbon steel surface was observed, following the Freundlich adsorption isotherm. PP measurements indicated that the studied extracts function as mixed-type inhibitors. SEM-EDS analysis further demonstrated enhanced surface homogeneity upon inhibitory introduction, particularly with NP addition, showcasing decreased Fe and Cl weight percentages alongside increased oxygen and carbon, suggesting the formation of a protective barrier by inhibitory molecules on the carbon steel surface. Spectrophotometric analysis revealed reduced polyphenol levels in corrosion products, while the intensity of Fe^{2+} decreased with increasing inhibitory concentrations, illustrating the corrosion-inhibitive action of the studied extracts.

Data Availability

The data used to support the findings of this study are included within the article.

Conflicts of Interest

The authors declare that they have no conflicts of interest.

Acknowledgments

The authors are grateful to Echahid Cheikh Larbi Tebessi University for providing facilities for the realization of this work.

References

[1] T. A. Salman, Q. A. Jawad, M. A. Hussain et al., "New environmental friendly corrosion inhibitor of mild steel in hydrochloric acid solution: adsorption and thermal studies," *Cogent Engineering*, vol. 7, no. 1, p. 1826077, 2020.

[2] O. Dagdag, Z. Safi, H. Erramli et al., "Epoxy prepolymer as a novel anti-corrosive material for carbon steel in acidic solution: electrochemical, surface and computational studies," *Materials Today Communications*, vol. 22, 2020.

[3] M. A. Bidi, M. Azadi, and M. Rassouli, "A new green inhibitor for lowering the corrosion rate of carbon steel in 1 M HCl solution: hyalomma tick extract," *Materials Today Communications*, vol. 24, 2020.

[4] A. Shahmoradi, N. Talebibahmanbigloo, C. Nickhil et al., "Molecular-MD/atomic-DFT theoretical and experimental studies on the quince seed extract corrosion inhibition performance on the acidic-solution attack of mild-steel," *Journal of Molecular Liquids*, vol. 346, 2022.

[5] A. A. Al-Amiery, A. B. Mohamad, A. A. H. Kadhum, L. M. Shaker, W. N. R. W. Isahak, and M. S. Takriff, "Experimental and theoretical study on the corrosion inhibition of mild steel by nonanedioic acid derivative in hydrochloric acid solution," *Scientific Reports*, vol. 12, pp. 4705–4721, 2022.

[6] A. Salcı, H. Yüksel, and R. Solmaz, "Experimental studies on the corrosion inhibition performance of 2-(2-aminophenyl) benzimidazole for mild steel protection in HCl solution," *Journal of the Taiwan Institute of Chemical Engineers*, vol. 134, 2022.

[7] O. M. A. Khamaysa, I. Selatnia, H. Zeghache et al., "Enhanced corrosion inhibition of carbon steel in HCl solution by a newly synthesized hydrazone derivative: mechanism exploration from electrochemical, XPS, and computational studies," *Journal of Molecular Liquids*, vol. 315, 2020.

[8] O. Fergachi, F. Benhiba, M. Rbaa et al., "Corrosion inhibition of ordinary steel in 5.0 M HCl medium by benzimidazole

derivatives: electrochemical, UV–visible spectrometry, and DFT calculations," *Journal of Bio- and Tribo-Corrosion*, vol. 5, pp. 21–13, 2019.

[9] M. Damej, S. Kaya, B. El Ibrahimi et al., "The corrosion inhibition and adsorption behavior of mercaptobenzimidazole and bis-mercaptobenzimidazole on carbon steel in 1.0 M HCl: experimental and computational insights," *Surfaces and Interfaces*, vol. 24, 2021.

[10] N. Arrousse, R. Salim, A. Abdellaoui et al., "Synthesis, characterization, and evaluation of xanthene derivative as highly effective, nontoxic corrosion inhibitor for mild steel immersed in 1 M HCl solution," *Journal of the Taiwan Institute of Chemical Engineers*, vol. 120, pp. 344–359, 2021.

[11] M. Afrokh, S. Baroud, Y. Kerroum et al., "Green approach to corrosion inhibition of carbon steel by fucus spiralis extract in 1 M HCl medium," *Biointerface Research in Applied Chemistry*, 2021.

[12] A. Dehghani, G. Bahlakeh, B. Ramezanzadeh, and M. Ramezanzadeh, "Potential of Borage flower aqueous extract as an environmentally sustainable corrosion inhibitor for acid corrosion of mild steel: electrochemical and theoretical studies," *Journal of Molecular Liquids*, vol. 277, pp. 895–911, 2019.

[13] Y. Wu, L. Guo, and Y. She, "Insight on the corrosion inhibition performance of psidium guajava linn leaves extract," *Journal of Molecular Liquids*, vol. 346, 2022.

[14] A. Kahlouche, H. Ferkous, A. Delimi et al., "Molecular insights through the experimental and theoretical study of the anticorrosion power of a new eco-friendly Cytisus multiflorus flowers extract in a 1 M sulfuric acid," *Journal of Molecular Liquids*, vol. 347, 2022.

[15] A. J. Rani, A. Thomas, M. Arshad, and A. Joseph, "The influence of aqueous and alcoholic extracts of Garcinia Cambogia fruit rind in the management of mild steel corrosion in hydrochloric acid: theoretical and electroanalytical studies," *Journal of Molecular Liquids*, vol. 346, 2022.

[16] I. Ogundana, A. Olalemi, and D. Arotupin, "Effect of aqueous extracts of leaves, stem and seed of Azadirachta indica on corrosion inhibition of mild steels in acidic medium," *Advanced Engineering Forum*, vol. 45, pp. 15–30, 2022.

[17] M. Deyab, Q. Mohsen, and L. Guo, "Theoretical, chemical, and electrochemical studies of Equisetum arvense extract as an impactful inhibitor of steel corrosion in 2 M HCl electrolyte," *Scientific Reports*, vol. 12, pp. 2255–2314, 2022.

[18] S. Boudiba, K. Hanini, I. Selatnia, A. Saouane, S. Hioun, and M. Benahmed, "Experimental, theoretical and mathematical studies of Echium italicum L. extract as a corrosion inhibitor for carbon steel in acidic medium," *Materials Research Express*, vol. 6, no. 8, p. 086546, 2019.

[19] K. Hanini, B. Merzoug, S. Boudiba, I. Selatnia, H. Laouer, and S. Akkal, "Influence of different polyphenol extracts of Taxus baccata on the corrosion process and their effect as additives in electrodeposition," *Sustainable Chemistry and Pharmacy*, vol. 14, 2019.

[20] O. T. Ogunmodede, "Duplex Stainless Steel 2101 corrosion inhibition in an acidic environment using Solanum tuberosum leaves and roots extract, Egypt," *Journal of Chemistry*, vol. 65, pp. 2–4, 2022.

[21] I. Ghazi, M. Zefzoufi, M. Siniti, R. Fdil, and H. Elattari, "Corrosion inhibition of carob pod pulp (ceratonia siliqua L.) on carbon steel surface C38 in hydrochloric acid," *Journal of Bio- and Tribo-Corrosion*, vol. 8, pp. 31–23, 2022.

[22] R. Aboorvakani, S. J. Kennady Vethanathan, and K. Madhu, "Influence of Zn concentration on zinc oxide nanoparticles and their anti-corrosion property," *Journal of Alloys and Compounds*, vol. 834, 2020.

[23] H. Chen, H. Fan, N. Su, R. Hong, and X. Lu, "Highly hydrophobic polyaniline nanoparticles for anti-corrosion epoxy coatings," *Chemical Engineering Journal*, vol. 420, 2021.

[24] S. Ramamoorthy, S. Surendhiran, D. Senthil Kumar et al., "Evaluation of photocatalytic and corrosion properties of green synthesized zinc oxide nanoparticles," *Journal of Materials Science: Materials in Electronics*, vol. 33, no. 12, pp. 9722–9731, 2022.

[25] G. M. Al-Senani, "Synthesis of ZnO-NPs using a Convolvulus arvensis leaf extract and proving its efficiency as an inhibitor of carbon steel corrosion," *Materials*, vol. 13, no. 4, p. 890, 2020.

[26] R. H. Al-Dahiri, A. M. Turkustani, and M. A. Salam, "The application of zinc oxide nanoparticles as an eco-friendly inhibitor for steel in acidic solution," *International Journal of Electrochemical Science*, vol. 15, no. 1, pp. 442–457, 2020.

[27] T. W. Quadri, L. O. Olasunkanmi, O. E. Fayemi, M. M. Solomon, and E. E. Ebenso, "Zinc oxide nanocomposites of selected polymers: synthesis, characterization, and corrosion inhibition studies on mild steel in HCl solution," *ACS Omega*, vol. 2, no. 11, pp. 8421–8437, 2017.

[28] A. Bendiabdellah, M. E. A. Dib, N. Meliani, N. Djabou, H. Allali, and B. Tabti, "Preliminary phytochemical screening and antioxidant activities of solvent extracts from Daucus crinitus Desf., from Algeria," *Journal of Applied Pharmaceutical Science*, vol. 2, pp. 92–95, 2012.

[29] A. Bendiabdellah, M. E. A. Dib, N. Meliani et al., "Antibacterial activity of*Daucus crinitus*Essential oils along the vegetative life of the plant," *Journal of Chemistry*, vol. 2013, Article ID 149502, 7 pages, 2013.

[30] D. Lanfranchi, H. Laouer, M. El-Kolli, S. Prado, C. Maulay-Bailly, and N. Baldovini, "Bioactive phenylpropanoids from Daucus crinitus desf. From Algeria," *Journal of Agricultural and Food Chemistry*, vol. 58, no. 4, pp. 2174–2179, 2010.

[31] M. Dib, M. Bendahou, A. Bendiabdellah et al., "Partial chemical composition and antimicrobial activity of Daucus crinitus Desf. extracts," *Grasas Y Aceites*, vol. 61, no. 3, pp. 271–278, 2010.

[32] H. karima, B. Sameh, B. Baya et al., "Corrosion inhibition impact of Pyracantha coccinea M. Roem extracts and their use as additives in zinc electroplating: coating morphology, electrochemical and weight loss investigations," *Journal of the Taiwan Institute of Chemical Engineers*, vol. 121, pp. 337–348, 2021.

[33] H. Beddiar, S. Boudiba, M. Benahmed et al., "Chemical composition, anti-quorum sensing, enzyme inhibitory, and antioxidant properties of phenolic extracts of clinopodium nepeta l. Kuntze," *Plants*, vol. 10, no. 9, p. 1955, 2021.

[34] K. Elumalai and S. Velmurugan, "Green synthesis, characterization and antimicrobial activities of zinc oxide nanoparticles from the leaf extract of Azadirachta indica (L.)," *Applied Surface Science*, vol. 345, pp. 329–336, 2015.

[35] G. Legwaila, W. Mojeremane, M. Madisa, R. Mmolotsi, and M. Rampart, "Potential of traditional food plants in rural household food security in Botswana," *Journal of Horticulture and Forestry*, vol. 3, pp. 171–177, 2011.

[36] H. Pyenson and P. Tracy, "A 1, 10—phenanthroline method for the determination of iron in powdered milk," *Journal of Dairy Science*, vol. 28, no. 5, pp. 401–412, 1945.

[37] M. Benahmed, I. Selatnia, N. Djeddi, S. Akkal, and H. Laouer, "Adsorption and corrosion inhibition properties of butanolic

extract of Elaeoselinum thapsioides and its synergistic effect with Reutera lutea (Desf.) Maires (Apiaceae) on A283 carbon steel in hydrochloric acid solution," *Chemistry Africa*, vol. 3, no. 1, pp. 251–261, 2020.

[38] N. B. Iroha and O. Akaranta, "Experimental and surface morphological study of corrosion inhibition of N80 carbon steel in HCl stimulated acidizing solution using gum exudate from Terminalia Mentaly," *SN Applied Sciences*, vol. 2, no. 9, pp. 1514–1611, 2020.

[39] S. Chaudhary and R. K. Tak, "Natural corrosion inhibition and adsorption characteristics of Tribulus terrestris plant extract on aluminium in hydrochloric acid environment," *Biointerface Research in Applied Chemistry*, vol. 12, pp. 2603–2617, 2022.

[40] Q. Wang, B. Tan, H. Bao et al., "Evaluation of Ficus tikoua leaves extract as an eco-friendly corrosion inhibitor for carbon steel in HCl media," *Bioelectrochemistry*, vol. 128, pp. 49–55, 2019.

[41] H. Derfouf, Y. Harek, L. Larabi, W. J. Basirun, and M. Ladan, "Corrosion inhibition activity of carbon steel in 1.0 M hydrochloric acid medium using Hammada scoparia extract: gravimetric and electrochemical study," *Journal of Adhesion Science and Technology*, vol. 33, no. 8, pp. 808–833, 2019.

[42] N. J. Maduelosi and N. B. Iroha, "Insight into the adsorption and inhibitive effect of spironolactone drug on C38 carbon steel corrosion in hydrochloric acid environment," *Journal of Bio- and Tribo-Corrosion*, vol. 7, pp. 6–14, 2021.

[43] A. Idress and D. M. Ibrahim, "Research article inhibition effect of benzylpenicillin drug towards corrosion of carbon steel in acidic solutions," *Current Research in Chemical*, 2020.

[44] L. Guo, J. Tan, S. Kaya, S. Leng, Q. Li, and F. Zhang, "Multidimensional insights into the corrosion inhibition of 3, 3-dithiodipropionic acid on Q235 steel in H2SO4 medium: a combined experimental and in silico investigation," *Journal of Colloid and Interface Science*, vol. 570, pp. 116–124, 2020.

[45] J. Tan, L. Guo, D. Wu et al., "Electrochemical and computational studies on the corrosion inhibition of mild steel by 1-hexadecyl-3-methylimidazolium bromide in HCl medium," *International Journal of Electrochemical Science*, vol. 15, no. 3, pp. 1893–1903, 2020.

[46] D. Li, P. Zhang, X. Guo, X. Zhao, and Y. Xu, "The inhibition of mild steel corrosion in 0.5 MH 2 SO 4 solution by radish leaf extract," *RSC Advances*, vol. 9, no. 70, pp. 40997–41009, 2019.

[47] O. Ogunleye, A. Arinkoola, O. Eletta et al., "Green corrosion inhibition and adsorption characteristics of Luffa cylindrica leaf extract on mild steel in hydrochloric acid environment," *Heliyon*, vol. 6, no. 1, 2020.

[48] X. Wang, H. Jiang, D.-x. Zhang, L. Hou, and W.-j. Zhou, "Solanum lasiocarpum l. extract as green corrosion inhibitor for A3 steel in 1 M HCl solution," *International Journal of Electrochemical Science*, vol. 14, no. 2, pp. 1178–1196, 2019.

[49] A. Singh, K. Ansari, and M. Quraishi, "Inhibition effect of natural polysaccharide composite on hydrogen evolution and P110 steel corrosion in 3.5 wt% NaCl solution saturated with CO2: combination of experimental and surface analysis," *International Journal of Hydrogen Energy*, vol. 45, no. 46, pp. 25398–25408, 2020.

[50] A. Fawzy, M. Abdallah, M. Alfakeer, H. M. Altass, I. I. Althagafi, and Y. A. El-Ossaily, "Performance of unprecedented synthesized biosurfactants as green inhibitors for the corrosion of mild steel-37-2 in neutral solutions: a mechanistic approach," *Green Chemistry Letters and Reviews*, vol. 14, no. 3, pp. 488–499, 2021.

[51] R. A. Hameed, E. Aljuhani, A. Al-Bagawi, A. Shamroukh, and M. Abdallah, "Study of sulfanyl pyridazine derivatives as efficient corrosion inhibitors for carbon steel in 1.0 M HCl using analytical techniques," *International Journal of Corrosion and Scale Inhibition*, vol. 9, pp. 623–643, 2020.

[52] A. A. Abdulridha, M. A. Albo Hay Allah, S. Q. Makki, Y. Sert, H. E. Salman, and A. A. Balakit, "Corrosion inhibition of carbon steel in 1 M H2SO4 using new Azo Schiff compound: electrochemical, gravimetric, adsorption, surface and DFT studies," *Journal of Molecular Liquids*, vol. 315, 2020.

[53] M. Alfakeer, M. Abdallah, and A. Fawzy, "Corrosion inhibition effect of expired ampicillin and flucloxacillin drugs for mild steel in aqueous acidic medium," *International Journal of Electrochemical Science*, vol. 15, no. 4, pp. 3283–3297, 2020.

[54] A. Chaouiki, M. Chafiq, H. Lgaz et al., "Green corrosion inhibition of mild steel by hydrazone derivatives in 1.0 M HCl," *Coatings*, vol. 10, no. 7, p. 640, 2020.

[55] M. Abdallah, A. Fawzy, and M. Alfakeer, "Inhibition potentials and adsorption performance of two sulfonylurea antibiotic expired drugs on the corrosion of mild steel in 0.5 M H2SO4," *International Journal of Electrochemical Science*, vol. 15, no. 10, pp. 10289–10303, 2020.

[56] Y. E. Kacimi, R. Touir, K. Alaoui et al., "Anti-corrosion properties of 2-phenyl-4 (3H)-quinazolinone-substituted compounds: electrochemical, quantum chemical, Monte Carlo, and molecular dynamic simulation investigation," *Journal of Bio- and Tribo-Corrosion*, vol. 6, no. 2, pp. 47–25, 2020.

[57] H. Mahfoud, N. Rouag, S. Boudiba, M. Benahmed, K. Morakchi, and S. Akkal, "Mathematical and electrochemical investigation of lamium flexuosum extract as effective corrosion inhibitor for CS in acidic solution using multidimensional minimization program system," *Arabian Journal for Science and Engineering*, vol. 47, no. 5, pp. 6605–6616, 2022.

[58] A. Abdel-Gaber, H. Rahal, and F. Beqai, "Eucalyptus leaf extract as a eco-friendly corrosion inhibitor for mild steel in sulfuric and phosphoric acid solutions," *International Journal of Industrial Chemistry (IJIC)*, vol. 11, no. 2, pp. 123–132, 2020.

[59] R. S. Abdel Hameed, A. Al-Bagawi, H. A. Shehata, A. H. Shamroukh, and M. Abdallah, "Corrosion inhibition and adsorption properties of some heterocyclic derivatives on C-steel surface in HCl," *Journal of Bio- and Tribo-Corrosion*, vol. 6, no. 2, pp. 51–11, 2020.

[60] R. S. Abdel Hameed, "Schiff'bases as corrosion inhibitor for aluminum alloy in hydrochloric acid medium," *Tenside Surfactants Detergents*, vol. 56, no. 3, pp. 209–215, 2019.

[61] U. Pal, J. G. Serrano, P. Santiago, G. Xiong, K. Ucer, and R. J. O. M. Williams, "Synthesis and optical properties of ZnO nanostructures with different morphologies," *Optical Materials*, vol. 29, no. 1, pp. 65–69, 2006.

[62] U. Pal and P. Santiago, "Controlling the morphology of ZnO nanostructures in a low-temperature hydrothermal process," *Journal of Physical Chemistry B*, vol. 109, no. 32, pp. 15317–15321, 2005.

[63] R. Sharma, R. Garg, and A. Kumari, "A review on biogenic synthesis, applications and toxicity aspects of zinc oxide nanoparticles," *EXCLI Journal*, vol. 19, pp. 1325–1340, 2020.

[64] D. K. Verma, S. Kaya, E. Ech-chihbi, F. El-Hajjaji, M. M. Phukan, and H. M. Alnashiri, "Investigations on some coumarin based corrosion inhibitors for mild steel in aqueous acidic medium: electrochemical, surface morphological,

density functional theory and Monte Carlo simulation approach," *Journal of Molecular Liquids*, vol. 329, 2021.

[65] M. Yadav, S. Kumar, R. R. Sinha, I. Bahadur, and E. E. Ebenso, "New pyrimidine derivatives as efficient organic inhibitors on mild steel corrosion in acidic medium: electrochemical, SEM, EDX, AFM and DFT studies," *Journal of Molecular Liquids*, vol. 211, pp. 135–145, 2015.

[66] F. Benhiba, Z. Benzekri, A. Guenbour et al., "Combined electronic/atomic level computational, surface (SEM/EDS), chemical and electrochemical studies of the mild steel surface by quinoxalines derivatives anti-corrosion properties in 1 mol.L^{-1} HCl solution," *Chinese Journal of Chemical Engineering*, vol. 28, no. 5, pp. 1436–1458, 2020.

[67] A. O. James and N. B. Iroha, "New green inhibitor of *Olax subscorpioidea* root for J55 carbon steel corrosion in 15% HCl: theoretical, electrochemical, and surface morphological investigation," *Emergent Materials*, vol. 5, no. 4, pp. 1119–1131, 2021.

[68] A. Ostovari, S. M. Hoseinieh, M. Peikari, S. R. Shadizadeh, and S. J. Hashemi, "Corrosion inhibition of mild steel in 1 M HCl solution by henna extract: a comparative study of the inhibition by henna and its constituents (Lawsone, Gallic acid, α-D-Glucose and Tannic acid)," *Corrosion Science*, vol. 51, no. 9, pp. 1935–1949, 2009.

[69] X. Li, S. Deng, H. Fu, and X. Xie, "Synergistic inhibition effects of bamboo leaf extract/major components and iodide ion on the corrosion of steel in H_3PO_4 solution," *Corrosion Science*, vol. 78, pp. 29–42, 2014.

[70] S. Deng and X. Li, "Inhibition by *Jasminum nudiflorum* Lindl. leaves extract of the corrosion of aluminium in HCl solution," *Corrosion Science*, vol. 64, pp. 253–262, 2012.

[71] N. Soltani, N. Tavakkoli, M. Khayatkashani, M. R. Jalali, and A. Mosavizade, "Green approach to corrosion inhibition of 304 stainless steel in hydrochloric acid solution by the extract of *Salvia officinalis* leaves," *Corrosion Science*, vol. 62, pp. 122–135, 2012.

[72] L. Huang, S. S. Wang, H. J. Li, J. Y. Wang, Z. G. Li, and Y. C. Wu, "Highly effective Q235 steel corrosion inhibition in 1M HCl solution by novel green strictosamide from *Uncaria laevigata*: experimental and theoretical approaches," *Journal of Environmental Chemical Engineering*, vol. 10, no. 3, 2022.

[73] A. Marsoul, M. Ijjaali, F. Elhajjaji, M. Taleb, R. Salim, and A. Boukir, "Phytochemical screening, total phenolic and flavonoid methanolic extract of pomegranate bark (*Punica granatum* L): evaluation of the inhibitory effect in acidic medium 1 M HCl," *Materials Today: Proceedings*, vol. 27, pp. 3193–3198, 2020.

[74] R. Haldhar, D. Prasad, A. Saxena, and P. Singh, "*Valeriana wallichii* root extract as a green and sustainable corrosion inhibitor for mild steel in acidic environments: experimental and theoretical study," *Materials Chemistry Frontiers*, vol. 2, no. 6, pp. 1225–1237, 2018.

[75] A. M. Eldesoky, A. S. Fouda, G. E. Bekheit, and N. S. Elsheikh, "Adsorption and corrosion inhibition of *alkanna tinctoria* extract (ATE) on copper in 1 M HNO_3 solution," *International Journal of Advanced Research*, vol. 3, pp. 991–1007, 2015.

[76] Z. Zhou, X. Min, S. Wan, J. Liu, B. Liao, and X. Guo, "A novel green corrosion inhibitor extracted from waste feverfew root for carbon steel in H2SO4 solution," *Results in Engineering*, vol. 17, 2023.

[77] M. Abdallah, H. M. Altass, B. A. Al Jahdaly, and M. M. Salem, "Some natural aqueous extracts of plants as green inhibitor for carbon steel corrosion in 0.5 M sulfuric acid," *Green Chemistry Letters and Reviews*, vol. 11, no. 3, pp. 189–196, 2018.

[78] H. M. Elabbasy, M. E. Elnagar, and A. E. S. Fouda, "Chemical, electrochemical, and surface studies of *Rosa damascene* extract as a green corrosion inhibitor for carbon steel in sulfuric acid environment," *Journal of the Chinese Chemical Society*, vol. 71, no. 4, pp. 385–396, 2024.

[79] N. Saigaa, S. Bouguessa, W. Boukhedena, M. Nacer, A. Nadji, and A. J. J. o.E. S. Gouasmia, "Engineering, Optimization of the inhibition corrosion of carbon steel in an acidic medium by a novel eco-friendly inhibitor *Asphodelus ramosus* using response surface methodology," *Journal of Electrochemical Science and Engineering*, vol. 13, pp. 469–490, 2023.

[80] A. Soudani, B. Harkati, A. Nadjem, and A. J. A. C. S. Gouasmia, "Corrosion inhibition behavior and adsorption mechanism of ethyl acetate extract from *scorzonera undulata* for carbon steel in 1 M HCl solution," *Acta Chimica Slovenica*, vol. 70, pp. 111–121, 2023.